Journal of Neuroscience Methods 253 (2015) 116–125

Contents lists available at ScienceDirect

Journal of Neuroscience Methods

journal homepage: www.elsevier.com/locate/jneumeth

Clinical neuroscience

Advanced target identification in STN-DBS with beta power of combined local field potentials and spiking activity

Rens Verhagen[a,*], Daphne G.M. Zwartjes[c], Tjitske Heida[c], Evita C. Wiegers[c], M. Fiorella Contarino[a,d], Rob M.A. de Bie[a], Pepijn van den Munckhof[b], P. Richard Schuurman[b], Peter H. Veltink[c], Lo J. Bour[a]

[a] Department of Neurology and Clinical Neurophysiology, Academic Medical Center, Meibergdreef 9, Amsterdam 1105 AZ, The Netherlands
[b] Department of Neurosurgery, Academic Medical Center, Meibergdreef 9, Amsterdam 1105 AZ, The Netherlands
[c] MIRA Institute for Biomedical Engineering and Technical Medicine, Biomedical Signals & Systems, University of Twente, Drienerlolaan 5, Enschede 7522 NB, The Netherlands
[d] Department of Neurology, Haga Teaching Hospital, Leyweg 275, Den Haag 2545 CH, The Netherlands

HIGHLIGHTS

- We simultaneously measure LFP and neuronal spiking in different areas of the STN.
- We use coherence between LFP and neuronal spiking to guide spectral power analysis.
- The 'coherence method' increases the difference in LFP beta power between STN areas.
- The 'coherence method' minimizes the influence of volume conduction on LFP analysis.

ARTICLE INFO

Article history:
Received 23 December 2014
Received in revised form 5 June 2015
Accepted 8 June 2015
Available online 12 June 2015

Keywords:
Deep brain stimulation
Parkinson's disease
Subthalamic nucleus
Local field potential
Neuronal spiking activity
Coherence

ABSTRACT

Background: In deep brain stimulation of the subthalamic nucleus (STN-DBS) for Parkinson's Disease (PD), often microelectrode recordings (MER) are used for STN identification. However, for advanced target identification of the sensorimotor STN, it may be relevant to use local field potential (LFP) recordings. Then, it is important to assure that the measured oscillations are coming from the close proximity of the electrode.

New method: Through multiple simultaneous recordings of LFP and neuronal spiking, we investigated the temporal relationship between local neuronal spiking and more global LFP. We analyzed the local oscillations in the LFP by calculating power only over specific frequencies that show a significant coherence between LFP and neuronal spiking. Using this 'coherence method', we investigated how well measurements in the sensorimotor STN could be discriminated from measurements elsewhere in the STN.

Results/comparison with existing methods: The 'sensorimotor power index' (SMPI) of beta frequencies, representing the ability to discriminate sensorimotor STN measurements based on the beta power, was significantly larger using the 'coherence method' for LFP spectral analysis compared to other methods where either the complete LFP beta spectrum or only the prominent peaks in the LFP beta spectrum were used to calculate beta power.

Conclusions: The results suggest that due to volume conduction of beta frequency oscillations, proper localization of the sensorimotor STN with only LFP recordings is difficult. However, combining recordings of LFP and neuronal spiking and calculating beta power over the coherent parts of the LFP spectrum can be beneficial in discriminating the sensorimotor STN.

1. Introduction

Deep brain stimulation of the subthalamic nucleus (STN-DBS) has emerged as an effective surgical treatment for Parkinson's disease (PD) (Benabid et al., 2009; Deuschl et al., 2006; Odekerken et al., 2013; Weaver et al., 2009), although the underlying working

Abbreviations: MU-ST, Multiple unit spike train; SMPI, Sensorimotor power index.

* Corresponding author. Tel.: +31 20 5668417.
E-mail address: r.verhagen@amc.uva.nl (R. Verhagen).

http://dx.doi.org/10.1016/j.jneumeth.2015.06.006
0165-0270/

mechanisms of DBS still are not fully understood. A leading hypothesis is that DBS suppresses pathological synchronized oscillations in the basal ganglia (Brown and Eusebio, 2008; Eusebio et al., 2012). Besides the favorable therapeutic effects, STN-DBS may also be accompanied by side effects, including side effects on cognition, behavior, and mood (Temel et al., 2006; Witt et al., 2008). It is thought that side effects are avoided and therapeutic effects of DBS are improved by selectively stimulating the dorsolateral STN (Lourens et al., 2013; Mallet et al., 2007; Saint-Cyr et al., 2002; Ulla et al., 2011; Voges et al., 2002; Yelnik et al., 2003) which is the area of the STN predominantly associated with sensorimotor function (Hamani et al., 2004; Parent and Hazrati, 1995; Temel et al., 2005). In this regard, the challenging task in DBS surgery is to locate not only the borders of the STN, but especially its sensorimotor area.

In addition to the standard T2 MRI-based targeting, some centers are using intraoperative recordings with microelectrodes (MER) to identify STN activity. Through the interpretation of local neuronal spiking activity measured with MER, electrode placement is guided and it allows the neurosurgeon to functionally refine targeting (Amirnovin et al., 2006; Bour et al., 2010; Schlaier et al., 2013). It may be relevant to further fine-tune targeting based on local field potential (LFP) recordings from the same electrodes or even from the contact points of the implanted DBS lead. An additional possible advantage of using LFP signals to verify electrode placement could be that they can be measured from the implanted electrode even after surgery to continuously monitor the position of the DBS lead with respect to the STN, thereby providing feedback for the configuration of the stimulation parameters (Bakstein et al., 2012; Little et al., 2013; Priori et al., 2013; Winestone et al., 2012).

Disadvantages of using the LFP signal in this way are primarily the loss of spatial resolution due to the relatively large size of the electrodes and the inter-contact distance on the lead. Also, single unit or multiple unit spiking activity cannot be detected by these larger surface electrodes. When using the LFP signal one has to rely on low frequency oscillations of the background signal, for instance in the beta (12–35 Hz) and gamma (35–80 Hz) band, to localize the STN and its sensorimotor area.

Previous studies in PD have shown that neural activity in the beta frequency band, measured with LFP, has an increased power in the sensorimotor STN compared to other regions inside the STN and areas outside the STN (Chen et al., 2006; Contarino et al., 2012; Kühn et al., 2005; Trottenberg et al., 2007; Weinberger et al., 2006). Elevated synchronized beta activity is considered to be related to antikinetic motor activity and seems to be associated with bradykinesia and rigidity in PD (Brown, 2003; Eusebio et al., 2012; Kühn et al., 2006). It is suggested that beta oscillations promote tonic activity at the expense of voluntary movement and that beta oscillations are modulated by dopamine therapy (Brown, 2007; Jenkinson and Brown, 2011), which induces a shift in the power spectrum of LFP activity, decreasing the spectral beta power and increasing the spectral power in the gamma frequency band (Alegre et al., 2005; Androulidakis et al., 2007; Cassidy et al., 2002; Fogelson et al., 2005; Williams et al., 2002).

With respect to synchronized gamma oscillations of LFP in the STN, it is thought that they have a physiological rather than a pathological origin and possibly relate to specific movement parameters since elevated gamma power is found before and during the execution of movements (Androulidakis et al., 2007; Brown, 2003; Brown and Williams, 2005; Cassidy et al., 2002). In a study by Trottenberg et al. (2006) in PD patients, gamma oscillatory activity measured with LFP was found to be increased in the zona incerta and the dorsal STN. Furthermore, Weinberger et al. (2009), found LFP power in the gamma frequency range to be increased when comparing periods of stronger tremor with periods of weaker tremor. These sites of increased gamma oscillations were mostly located in the dorsal part of the STN.

One of the challenges in identifying these specific oscillations in the STN and its sensorimotor area is to assure that the measured LFP signal is indeed coming from the close proximity of the electrode. The electric field produced by the slow oscillations represented in the LFP is conducted through the neuronal tissue. As a result, LFP measurements can be influenced by oscillating sources up to a distance of 10 mm depending on the conductive medium, the frequency of the oscillation (Juergens et al., 1999; Kajikawa and Schroeder, 2011; Mitzdorf, 1987), the architecture of the neural tissue as well as the amount of synchronization between the neural ensembles (Buzsaki et al., 2012). This is in contrast to the neuronal spiking activity represented in the MER signal, which can only come from neurons within a range of 100–200 μm around the microelectrode (Henze et al., 2000). Therefore, a way to verify the local nature of LFP oscillations can be by demonstrating that they correlate with local neuronal firing (Buzsaki et al., 2012).

The temporal relationship between LFP and neuronal spiking activity in the STN has not been widely studied. Alavi et al. (2013), found that 46% of STN neurons showed beta oscillatory spiking activity coherent with LFP. Weinberger et al. (2006), showed that 28% of recordings of spiking activity displayed significant oscillations in the beta frequencies of which the majority was localized in the dorsal STN. Almost all of these oscillating recordings were significantly coherent with LFP activity. In a study by Kühn et al. (2005), spike triggered averages (STA) of the LFP were used to show that the beta range oscillatory activity in the LFP was time-locked to the neuronal discharge with STA amplitudes being larger in the dorsal STN than in the ventral STN. In light of these results, beta LFP activity is not thought to be caused by oscillatory firing of STN neurons, but more likely to be the result of oscillatory afferent input into the neurons from outside the STN (Kühn et al., 2005; Weinberger et al., 2006).

In the current study, we have investigated a method to assess the temporal relationship between strictly local neuronal spiking activity measured with MER and more global neuronal activity measured with LFP recordings inside different functional parts of the STN. By simultaneously measuring LFP and neuronal spiking activity from the microelectrodes used in standard DBS surgery, we were able to study coherence between LFP and neuronal spiking activity and spectral power of both LFP and neuronal spiking on numerous positions across the subthalamic area with only a minimal change in the standard surgical procedures.

The local nature of oscillations in the LFP beta and gamma band was verified by analyzing specifically those frequencies in the LFP that show a significant coherence with local neuronal firing (i.e. LFP-spiking coherence passing the 99% confidence interval). We have compared this method with other frequently used methods spectral analysis. In this way, we have explored how the temporal coupling between neuronal spiking and LFP can guide spectral analysis and how combined recordings of LFP and neuronal spiking can be used for the localization of the sensorimotor part of the STN.

Both the beta and the gamma power of the LFP and neuronal spiking signals are hypothesized to be greater inside than outside the sensorimotor STN. Furthermore, we hypothesize that the analysis of spectral power around frequencies that show significant coherence between LFP and local neuronal firing can increase this difference and thereby help to discriminate between measurements inside and outside the sensorimotor STN.

2. Materials and methods

2.1. Participants and surgery

The study was approved by the Medical Ethical Committee of the Academic Medical Center in Amsterdam. All the subjects received

Table 1
Clinical characteristics (mean ± SD, [range]) of the PD patients included in this study.

Number of patients	25
Gender (women/men)	6/19
Age (years)	60 ± 10, [38–76]
Disease duration (years)	13 ± 7, [6–32]
Total UPDRS* III off drugs score	41 ± 10, [25–62]
Number of sides	48
Number of microelectrodes per STN	3 ± 1, [1–5]

* UPDRS = Unified Parkinson's Disease Rating Scale.

oral and written information and signed an informed consent prior to inclusion. The study was conducted conform the Declaration of Helsinki (1964 and later revisions), in accordance with the Dutch Act on Medical Research Involving Human Subjects (WMO) and with the Standard EN ISO 14155: 2011 on clinical investigation of medical devices for human subjects–Good Clinical Practice.

Twenty-five patients with idiopathic PD (age 60 ± 10 years) who underwent DBS surgery were included in this study. Twenty-three patients underwent bilateral STN-DBS and two patients had unilateral STN-surgery (Table 1). The selected patients – despite optimal drug treatment – suffered from severe response fluctuations, dyskinesias, painful dystonia and/or bradykinesia. Exclusion criteria were an age below 18 years, a Hoehn and Yahr stage of five at the best moment of the day, a Mattis dementia rating scale score of 120 or below, psychosis, and the general contra-indications for stereotactic surgery.

The procedure for DBS was a one-stage bilateral or unilateral stereotactic approach. A detailed description of the surgical procedures has been published before (Contarino et al., 2012). Standard MER was performed to determine the STN borders during DBS surgery using one to five steel cannulas and microelectrodes (FHC, Inc., Bowdoin, ME, USA) arranged in a cross shaped array with an inter-electrode distance of 2 mm.

2.2. Recording protocol

The number of microelectrodes was determined by the neurosurgeon, mainly based on the preoperative imaging. The recordings started 6 mm before the preoperatively determined MRI-based target point, and was continued downward in 0.5 mm steps until substantia nigra activity was recognizable in at least one channel or STN activity significantly decreased in all channels indicating the lower border of the STN. Standard MER was performed with the Leadpoint system (Medtronic, Minneapolis, MN, USA), amplified with a gain of 10,000, analog bandpass filtered between 500 and 5000 Hz (23 dB; 12 dB/oct). The signal was sampled at 12 kHz, by use of a 16-bit AD converter and afterwards up-sampled to 24 kHz off-line. Following a two seconds signal stabilization period after electrode movement cessation, multi-unit segments were recorded for 5–20 s. The MER signals were scored as recorded inside or outside the STN by an experienced physicist and a neurologist based on the observed combination of neuronal spiking activity and background noise (Bour et al., 2010; Cagnan et al., 2011).

At each depth, standard MER was immediately followed by a simultaneous recording of LFP and single/multi-unit activity using a switch board to connect the same microelectrodes to a different amplifier, suited for both high and low frequency signals (REFA amplifier, TMSi, Oldenzaal, the Netherlands). The recordings from the 10 μm exposure micro-tip were referenced against the 1 mm exposed surface of the inner cannula located 10 mm above the tip of the microelectrode and were sampled at 20 kHz. For the purpose of this study, recordings of 10 s (22 sides) or 15 s (26 sides) per depth were made. This short measurement time was chosen as it was assumed that this time window provided a sufficient representation of the STN activity, while keeping the additional surgery time as short as possible. Further processing and data analysis were performed off-line using MATLAB (v. 7.14, R2012a, The Mathworks, Natik, MA, USA).

2.3. Mapping procedure

Multiple recordings were made inside and outside the STN. In order to discriminate between measurements in the sensorimotor area and the non-sensorimotor area of the STN, we used a novel approach to map an atlas-derived 3D body of the STN on the microelectrode recording sites (Lourens et al., 2013; Lujan et al., 2009). This 3-dimensional mapping method uses the classifications of the standard MER recordings with the Leadpoint system to estimate the location and orientation of the STN for each patient specifically. A 3D brain atlas was used in which the STN is represented as a three-dimensional polygon surface (Butson et al., 2007; Miocinovic et al., 2007). We used an optimization function to find the optimal position, rotation and scaling of the STN atlas relative to the stereotactic locations of the MER measurements. A more extensive description of this mapping procedure and the specific settings used during the procedure has been published earlier (Lourens et al., 2013). The optimization procedure results in a spatial representation of the STN as it is defined by the observed combination of neuronal spiking activity and background noise measured by the Leadpoint microelectrode recordings. For the purpose of this study, it was assumed that at least two microelectrode tracks were required to obtain a reliable estimation of the STN location. One STN was excluded from further analysis, since it was estimated by only one microelectrode track.

Based on the work of Parent and Hazrati (1995), we assumed the sensorimotor area of the STN to be the lateral 2/3rd of the dorsal portion of the rostral 2/3rd of this STN body and the caudal 1/3rd of this STN body. The non-sensorimotor STN was defined to be the 1/3rd ventral part and the 1/3rd medial tip of the rostral 2/3rd of this STN body (Benarroch, 2008; Hamani et al., 2004; Parent and Hazrati, 1995). All simultaneous LFP and MER measurements done with the experimental setup were then labelled based on their stereotactic location in these different functional subthalamic areas (Fig. 1).

2.4. Data analysis

2.4.1. Localization of the measurements

After the labeling of measurements to their corresponding locations, the measurements were divided into three areas per studied STN: (1) recorded dorsal to the STN, (2) inside the sensorimotor part of the STN and (3) inside the non-sensorimotor part of the STN (Fig. 1). Measurements of trajectories that missed the STN and measurements ventral to the STN were excluded from further analysis.

2.4.2. Artifact detection

Artifacts which interfered with the analysis, including movement of the wires, talking of the patient and other mechanical disturbances, were excluded using an extensive artifact detection procedure. First, drift was removed from the recording by subtraction of a fifth order polynomial fitted to the recorded signal. Any remaining offset was removed by high pass filtering the signal using a second order non-causal, zero-phase, Butterworth filter with a cut-off frequency of 0.5 Hz. Line noise was then removed using a second order non-causal, zero-phase, Butterworth band-stop filter between 48 Hz and 52 Hz.

To identify large amplitude artifacts and exclude them from further analysis, a visually assigned threshold was used on the instantaneous amplitude of the signal. The instantaneous amplitude was obtained by taking the real part of the Hilbert transform of the signal (Dolan et al., 2009). Subsequently, the periods in which

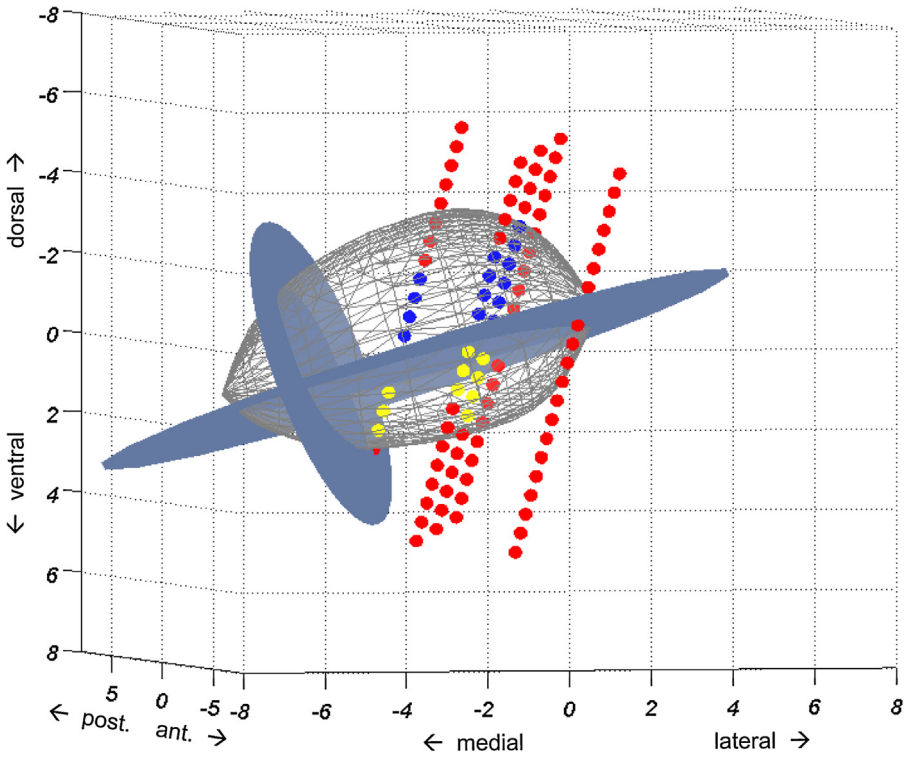

Fig. 1. A 3D view of the STN showing the results of the mapping procedure. The dots represent the MER measurement sites scored as outside (red) or inside (blue and yellow) of the STN. The gray body represents the atlas STN body fitted to the MER scorings by the optimization routine. The volume dorsolateral of the two oval blue planes is assumed to be the sensorimotor part of the STN. Based on these planes, the measurement sites inside the STN are divided into measurements in the sensorimotor part of the STN (blue) and in the non-sensorimotor part of the STN (yellow). (For interpretation of the references to color in this figure legend, the reader is referred to the web version of this article.)

this signal exceeded the visually assigned threshold and the 0.75 s before and after these periods were excluded from further analysis.

After the identification of large amplitude artifacts, further analysis was performed on the original waveform after offset removal and line noise filtering. The remaining periods of the recordings were divided into epochs of one second duration. Welch's method was used to calculate the power spectral density (PSD) of each one second epoch. For this, four 0.4 second windows with 50% overlap were averaged, resulting in a PSD with a frequency resolution of 2.5 Hz. These PSDs were further analyzed to detect artifacts in the one second epochs.

Two criteria were used for artifact detection in the one second epochs: First, the spectral power in both the 3–45 Hz and 55–95 Hz band of each epoch was not allowed to exceed four times the median spectral power in these frequency bands recorded in all epochs of a single recording. Second, to obtain a more reliable threshold in case many epochs of a single recording are influenced by artifacts, the spectral power of each epoch was also not allowed to exceed four times the median spectral power of all epochs recorded in the same neurological structure for one specific operation side (either inside or outside the STN). Epochs that did not meet both of these criteria were marked as artifacts and excluded from analysis. All remaining artifact-free segments of two or more consecutive seconds were used for further analysis.

2.4.3. Calculation of power spectra and coherence spectra of LFP oscillations and spike trains

Using different filters, two types of signals were obtained from the same measurement. The LFP signal was obtained by using a third order non-causal, zero-phase, Butterworth filter with band-pass frequencies between 3 Hz and 90 Hz. For analysis of the neuronal spiking activity, a spike train was retrieved from the high frequency component of the recording. For this, a third order non-causal, zero-phase, Butterworth filter with band-pass frequencies between 500 Hz and 3500 Hz was used. A spike train was created by marking local maxima of this signal as a spike event when the maxima exceeded 3.5 times the noise level estimated with the envelope method described before by Dolan et al. (2009). Spikes were ignored if the spike events occurred within 1 ms of each other (overlapping spikes), if the time between the positive and negative peak of the spike waveform exceeded 0.6 ms, if the amplitude of the negative peak was smaller than 0.3 times the amplitude of the positive peak, or if the amplitude of the positive peak was larger than 10 times the estimated noise level. This procedure has been described before in more detail (Lourens et al., 2013). The resulting multiple unit spike train (MU-ST) reflects the spiking activity of multiple neurons in close proximity of the micro-tip of the electrode (between 100 μm and 200 μm) (Grover and Buchwald, 1970; Henze et al., 2000; Moran and Bar-Gad, 2010). For accurate analysis of the beta and gamma frequencies in the spike trains, we assume that the MU-ST signal should contain at least one neuron spiking with a frequency of 12 Hz (start of the beta frequencies) or higher. Therefore, recordings with on average less than 12 spikes per second were excluded from further analysis. Despite the filtering of line noise, some recordings still showed a distinct 50 Hz peak in their PSD. Recordings for which the power between 48 and 52 Hz exceeded the sum of powers from 44 Hz to 48 Hz and from 52 to 56 Hz, were excluded from analysis as well.

Power spectral densities of the MU-ST and LFP signals and the spectral coherence between LFP and MU-ST were calculated using techniques described by Halliday et al. (1995). PSD and coherence were calculated over the complete artifact free part of the signal by taking into account the start samples and the lengths of each of the combined artifact free epochs. The combined artifact-free signal

had an average length of 10.7 s ±3.2 s (SD). The spectral estimation uses the average of the modulus squared Fourier transformation over 0.82 s non-overlapping segments (median of 12 segments per recording) resulting in a frequency resolution of 1.22 Hz. To account for possible differences in the electrodes used in different trajectories, normalization of the PSD was performed by dividing each PSD by the maximum power between 8 and 80 Hz measured in the same electrode trajectory.

2.4.4. Analysis of spectral power in the PSD of LFP oscillations and spike trains

In this study we compare three different methods to analyze the spectral powers in the beta and gamma frequency bands represented in the PSD of both the LFP and the MU-ST signals. For this purpose we analyze, using each of the three methods, the same PSD calculated out of the same artefact free parts of the same recordings.

In the first method, the power of the complete beta and gamma spectrum was calculated by integration of the PSD from 12 Hz to 35 Hz and 35 Hz to 80 Hz, respectively.

In the second method, a more commonly used method of PSD analysis was used where we detected the most prominent power peak within the beta and gamma range of the PSD for every recording. We did this by identifying the highest values within the beta and the gamma frequency ranges and integrating the PSD over a narrow frequency band (4.88 Hz) surrounding these single peaks for both the beta and the gamma frequency range.

As a third, novel experimental analysis, we introduced the 'coherence method' where the PSD was only integrated over a band surrounding the frequencies that show a significant coherence between the LFP and neuronal spiking activity reflected in the MU-ST signal (i.e. the frequencies for which the coherence spectrum passes the 99% confidence interval). This was done for both the beta (12–35 Hz) and gamma (35–80 Hz) range of the PSD individually. By using this coherence condition we make use of the correlation between the more globally measured LFP and neuronal spiking activity, which is known to be very local. Thereby we attempted to verify the local nature of the oscillations reflected in the LFP recordings. By minimizing the influence of beta and gamma frequency oscillations from distant sites, either those measured by the reference electrode or those spreading to the microelectrode through volume conduction, we limit the analysis of the LFP spectral power as much as possible to oscillating beta and gamma sources around the location of the micro-tip. To evaluate the 'coherence method' we introduced the 'sensorimotor power index' (SMPI), a measure representing the ability to discriminate between recordings in the sensorimotor and the non-sensorimotor area based on the mean spectral power in both areas:

$$\text{Sensorimotor power index(SMPI)} = \frac{\text{mean power in sensorimotor STN}}{\text{mean power in non-sensorimotor STN}} \quad (1)$$

In this equation, the mean power in a specific STN area is calculated by taking the average power of all the measurements localized in that area by the mapping procedure, that remained after artefact correction and spike train creation. When using the 'coherence method', measurements that showed no significant coherence between LFP and MU-ST in a specific frequency band were treated as measurements with zero spectral power in that frequency band. The SMPI values were calculated for both the LFP and the MU-ST signal and both using the beta and the gamma range of the power spectrum.

2.5. Statistics

Paired two-tailed *t*-tests were used to compare the percentage of measurements that showed a significant coherence between areas, for both the beta and gamma frequency ranges. We also compared the bandwidth over which the coherence spectrum passes the 99% confidence interval between areas, using paired two-tailed *t*-tests.

For the statistical analysis of the SMPI values, all results were logarithmically transformed, since the log of a ratio has better statistical properties than the ratio itself. One sample two-tailed *t*-tests, including Bonferroni correction for multiple comparisons ($n = 12$), were performed to test whether the log-transformed SMPI values were greater than zero, reflecting the hypothesized increased power in the sensorimotor STN. Paired two-tailed *t*-tests, including Bonferroni correction for multiple comparisons ($n = 12$), were performed to compare the log(SMPI) between the three methods used, for beta and gamma frequencies of both the LFP and the MU-ST signal.

The log(SMPI) is hypothesized to be greater than zero for both beta and gamma powers. The log(SMPI) values are hypothesized to be larger when using the 'coherence method' compared to the other two methods of spectral analysis, representing a better discrimination between the sensorimotor and the non-sensorimotor STN.

3. Results

After artefact correction, 44 sides (24 patients) showed enough stable recordings of adequate length to calculate reliable measures for power and coherence. Three sides had no artefact free measurements longer than two seconds in one (2 sides) of both (1 side) of the STN areas and the SMPI could therefore not be calculated. On one side, the depth of the recordings could not be confirmed with certainty and this side was also excluded.

The first two columns of Fig. 2 show one second examples of the LFP and the MU-ST signals that were simultaneously recorded in one channel, passing through the STN. The third column shows the coherence spectrum of the signals in the first two columns for measurements that show enough spikes to be suited for coherence analysis. The mapping procedure divided all the measurements into three area categories per STN.

3.1. Coherence between LFP and MU-ST

Table 2 shows the percentage of measurements that were used for coherence analysis after artifact correction and spike train creation. Because only a small percentage of the measurements dorsal to the STN shows spiking activity, the percentage of measurements that could be used for coherence analysis in that area was much smaller than in the sensorimotor and non-sensorimotor STN areas. The amount of measurements outside the STN that could be used for coherence analysis proved to be too small to make any statements about the added value of coherence in the analysis of the spectral powers. Therefore, this area category was not further analyzed.

Comparing the sensorimotor and the non-sensorimotor area, paired *t*-tests showed no significant differences in the percentage of measurements that show a beta coherence (42.1% vs 42.0%; $p = 0.99$), nor in those that show a gamma coherence (62.8% vs 68.4%; $p = 0.10$) (Table 2). However, the average bandwidth over which the beta coherence spectrum passed the 99% confidence interval was significantly larger in the sensorimotor area than in the non-sensorimotor area (4.5 Hz vs 3.6 Hz; $p = 0.005$). In the gamma coherence spectrum, no significant difference in the bandwidth of coherence was observed.

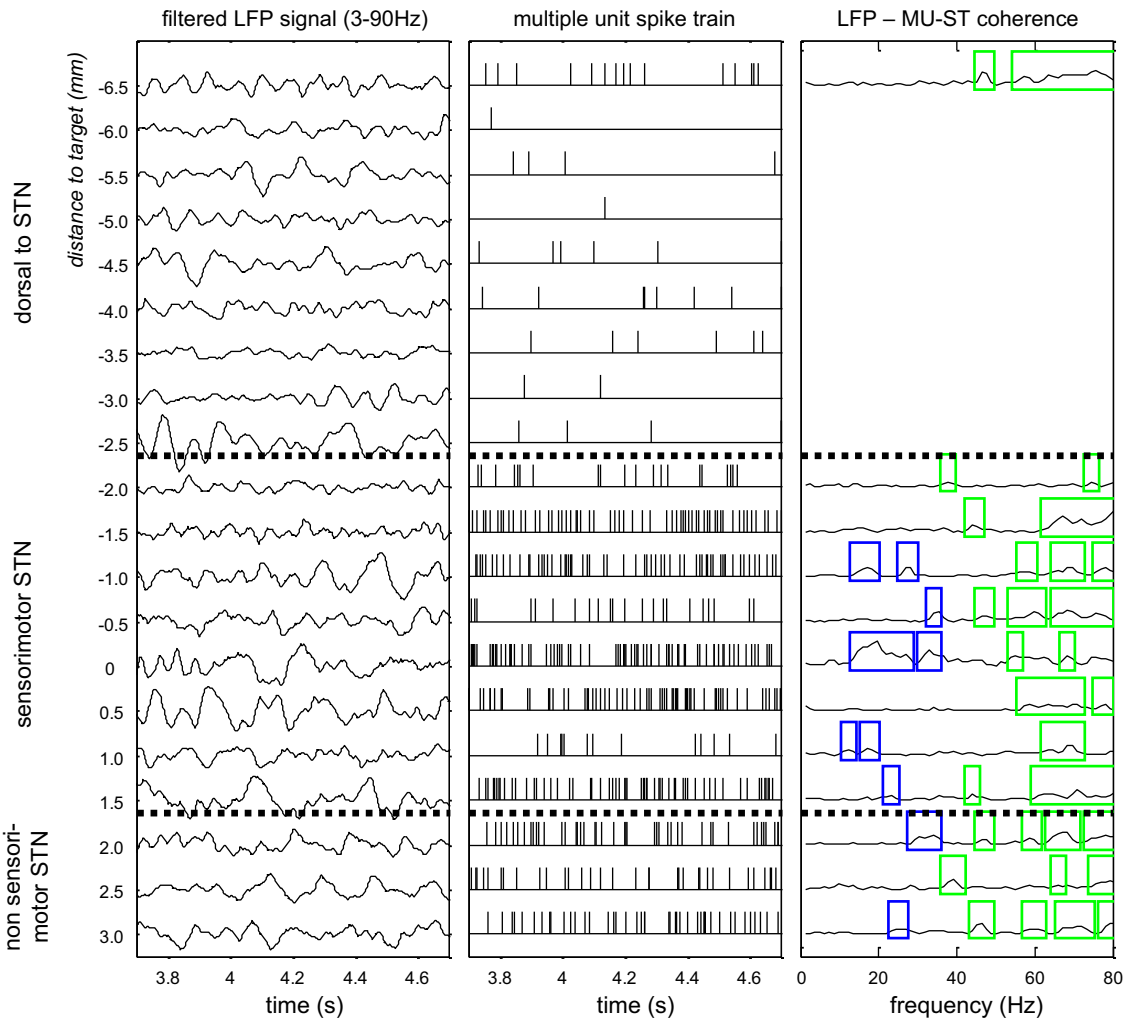

Fig. 2. Example of the LFP (left) and the MU-ST (middle) signals, simultaneously recorded in one channel, passing the three area categories indicated on the far left axis. The *y*-axis shows the distance in mm to the pre-defined target in the center of the STN. On the right the spectrum of the coherence between LFP and MU-ST is depicted for measurements that show enough spikes to be suited for coherence analysis. Blue and green rectangles represent frequency bands within the beta and gamma frequencies respectively for which the coherence between LFP and MU-ST passes the 99% confidence interval. (For interpretation of the references to color in this figure legend, the reader is referred to the web version of this article.)

3.2. Spectral power of the LFP and MU-ST

A summary of the logarithmically transformed SMPI values is shown in Table 3.

Both when calculating the spectral beta power using the complete beta spectrum from 12 Hz to 35 Hz and when calculating the power around the detected peaks in the beta spectrum, we found the log(SMPI) of the LFP beta frequencies to be significantly greater than zero, with mean = 0.085, $p < 0.001$ and mean = 0.089, $p < 0.001$, respectively. Also when using the 'coherence method', the log(SMPI) of the LFP beta frequencies was significantly greater than zero (mean = 0.262, $p < 0.001$). The average log(SMPI) of the LFP gamma frequencies was not significantly different from zero using any of the three methods of spectral analysis (Table 3).

Using the same methods for SMPI calculation on the MU-ST spectral density we found that both analyzing the complete beta power spectrum and analyzing power around detected peaks in the beta spectrum did not result in log(SMPI) values different from zero (mean = 0.108 and mean = 0.119, respectively). However, when using the 'coherence method', the log(SMPI) was significantly greater than zero, with mean = 0.335, $p = 0.001$. In the gamma frequencies, none of the three methods of MU-ST

Table 2
Overview of the amount of measurements per STN remaining in the three area categories after artifact correction (column 1), the percentage of these measurements that was suited for coherence analysis (column 2) and the percentage of these measurements with a significant coherence in the beta (column 3) and gamma (column 4) frequency bands.

	Average number of measurements per STN	Average percentage of measurements suited for coherence analysis (±SD)	Average percentage of measurements with significant beta coherence (±SD)	Average percentage of measurements with significant gamma coherence (±SD)
Dorsal to STN	18.4 (±9.9)	7.4%[a]		
Sensorimotor STN	20.5 (±5.3)	68.9% (±19.2)	42.1% (±13.5)	62.8% (±19.1)
Non-sensorimotor STN	8.3 (±3.2)	74.7% (±16.5)	42.0% (±17.0)	68.4% (±18.3)

[a] Median percentage (distribution of the percentages was skewed to the right).

Table 3
Overview of the mean log(SMPI) values calculated with the three different methods for LFP and MU-ST signals, for beta and gamma frequencies; *p*-values are depicted for the one sample *t*-tests comparing the mean log(SMPI) values to a value of zero.

	Complete spectrum analysis	Peak detection method	Coherence method
log(SMPI) beta LFP	0.085 (**$p < 0.001$**)	0.089 (**$p < 0.001$**)	0.262 (**$p < 0.001$**)
log(SMPI) gamma LFP	0.016 *not significant*	0.017 *not significant*	0.001 *not significant*
log(SMPI) beta MU-ST	0.108 *not significant*	0.119 *not significant*	0.335 (**$p = 0.001$**)
log(SMPI) gamma MU-ST	0.030 *not significant*	0.024 *not significant*	0.050 *not significant*

spectral analysis resulted in average log(SMPI) values that were significantly different for zero (Table 3).

Fig. 3 shows a graphic display of the log(SMPI) values of the LFP and MU-ST beta frequencies, including the results of paired *t*-tests comparing the log(SMPI) values between the three methods of spectral analysis.

Comparing the log(SMPI) values of LFP signals, no significant differences were found between the analysis of the complete spectrum and the analysis of power around detected PSD peaks. However, the 'coherence method' resulted in a significantly larger log(SMPI), both compared to the analysis of the complete spectrum as well as the analysis using peak detection in the PSD ($p < 0.001$)

A similar trend was observed when comparing the log(SMPI) values of MU-ST signals, though less significant. Analysis of the complete MU-ST spectrum and the analysis of power around detected peaks in the spectrum did not result in significantly different log(SMPI) values. Using the 'coherence method' seems to result in higher log(SMPI) values compared to both the other two methods of spectral analysis. However, when using Bonferroni correction for multiple comparisons ($n = 12$), the trend does not reach significance ($p = 0.016$ and $p = 0.025$ for comparison with complete spectrum analysis and peak detection analysis, respectively).

We found no significant differences when comparing the log(SMPI) values found using the gamma frequencies between methods, neither for LFP, nor for MU-ST signals.

4. Discussion

The results of this study suggest that, taking into account the coherence between LFP and MU-ST can help to differentiate measurements inside the sensorimotor STN from measurements elsewhere in the STN through the analysis of LFP spectral power in the beta band.

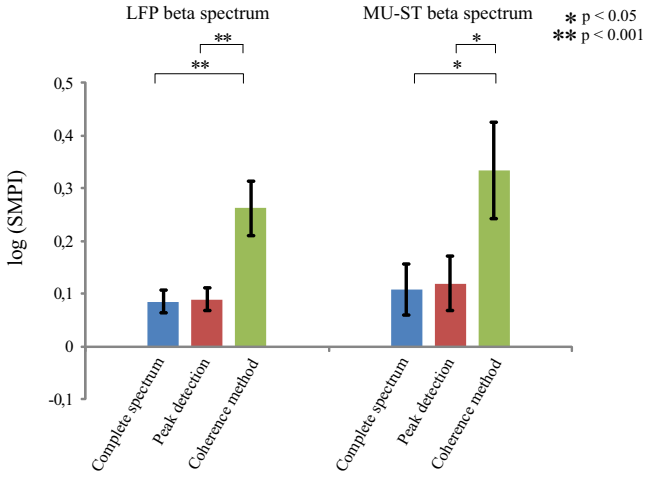

Fig. 3. Overview of the mean log(SMPI) values including standard errors of the means calculated by the three different methods of spectral analysis using the beta frequencies, for both LFP and MU-ST signals; *p*-values are depicted for the results of paired *t*-tests comparing log(SMPI) values between methods.

4.1. Coherence between LFP and MU-ST

The percentage of measurements that show a significant coherence between the LFP and MU-ST signals in the beta frequencies in this study is in accordance with the literature on this subject. We found significant coherence in 42.1% and 42.0% of measurements in sensorimotor and non-sensorimotor STN, respectively. Other studies report similar values of 46% (Alavi et al., 2013) and 25% (Weinberger et al., 2006) for the whole STN. These percentages probably relate to the percentage of oscillatory spiking neurons in the STN. Weinberger et al. (2006) have shown that almost all (89%) of the measurements that display oscillatory spiking activity, are coherent with simultaneously measured LFP.

Weinberger et al. (2006) report that most of the oscillatory neuronal spiking activity was found in the dorsal STN while Alavi et al. (2013) report no differences in localization. The latter is in accordance with our finding that the percentage of coherent measurements does not differ between sensorimotor STN and non-sensorimotor STN. In this study, the bandwidth over which the coherence between LFP and MU-ST passes the 99% confidence interval is larger inside than outside the sensorimotor STN (4.5 Hz vs 3.6 Hz; $p = 0.005$). However, the calculation of the coherence spectrum has a frequency resolution of only 1.22 Hz. Therefore, it is difficult to draw any conclusions from this minor difference in coherence bandwidth. It could potentially indicate that the MU-ST signal is a summation of multiple neurons oscillating in a broad range of beta frequencies, all coherent with similar beta frequencies in the LFP signal. This leads to a broader spectrum of coherent oscillations. This summation of multiple oscillating neurons in the MU-ST signal is more likely to occur inside the sensorimotor part of the STN, because oscillating neurons there may be more abundant (Weinberger et al., 2006). We believe that more research into the bandwidth of spiking frequencies in the beta range is necessary.

4.2. Spectral power of the LFP

The results of the current study confirm our hypothesis that LFP beta power is elevated in the sensorimotor part of the STN. An average log(SMPI) value greater than zero is found using all methods of LFP spectral analysis. However, the coherence method resulted in a significantly higher beta log(SMPI) value than the other two methods.

The increased LFP beta power in the sensorimotor STN compared to the non-sensorimotor STN is in accordance with previous studies (Chen et al., 2006; Contarino et al., 2012; Kühn et al., 2005; Lourens et al., 2013; Trottenberg et al., 2007; Weinberger et al., 2006). The significantly larger log(SMPI) when using the coherence method compared to the two other methods of LFP spectral analysis is probably due to the diminished influence of volume conducted oscillations in the beta frequencies.

How LFP signals are generated is rather complex (Moran and Bar-Gad, 2010). It is dominated by synaptic activity, but it is also influenced by several other processes, for example Ca^{2+} spikes, membrane oscillations, action potentials and spike hyperpolarizations (Buzsaki, 2002; Buzsaki et al., 2012; Goto and O'Donnell, 2001; Logothetis, 2002, 2003; Pedemonte et al., 1998). The dipoles and

return currents created by these processes together determine the extracellular field. One of the factors influencing the conductivity of this electric field is the dendritic morphology which acts as a low-pass filter (Linden et al., 2010). Therefore, the attenuation of slow oscillations over distance is relatively small and the low frequency LFP signal measured at the microelectrode tip may even reflect sources up to a distance of 10 mm (Juergens et al., 1999; Kajikawa and Schroeder, 2011; Mitzdorf, 1987). Volume conduction will thus play an important role in the measured LFP in the beta frequencies, especially inside a small structure like the STN.

On the contrary, spikes that are identifiable over the noise level in the high frequency signal are coming from neurons at a distance less than 150 μm around the microelectrode (Henze et al., 2000). The distance over which spikes are measureable is limited because of the fast attenuation of these high frequency signals (Legatt et al., 1980).

By limiting our power analysis to those frequencies that show a significant coherence between the LFP and the MU-ST signals, we diminish the contribution of oscillations in the beta frequency range that are coming from sources located either in different areas of the STN or outside the STN. This confinement to local oscillating sources is in contrast to the analysis of the complete spectrum, in which distant sources can be represented. Even PSD peak detection analysis, which is used to obtain the most prominent oscillating source in the signal, does not ensure that this prominent oscillation is indeed coming from the close proximity of the electrode, making it unreliable for the identification of the sensorimotor part of the STN.

Our hypothesis that LFP spectral power around significant gamma peaks in the coherence spectrum between LFP and MU-ST will discriminate better between the sensorimotor area and the non-sensorimotor area of the STN cannot be confirmed. Gamma log (SMPI) values for all three methods of LFP spectral analysis, including the coherence method, did not significantly differ from zero. Furthermore, no significant differences were found comparing the gamma log (SMPI) values between methods.

Gamma oscillations do not spread as far through the tissue as beta oscillations and thus volume conduction has a smaller effect on the power analysis of the gamma frequencies. Also, gamma oscillations are likely to show a more out-of-phase behavior over larger distances. This is reflected as an absence of clear peaks in the LFP power spectral density in the gamma range. Another reason for the absence of LFP gamma peaks could be that the patients in this study are measured during rest while gamma frequencies in the LFP are thought to relate more to specific movement parameters (Androulidakis et al., 2007; Brown, 2003; Brown and Williams, 2005; Cassidy et al., 2002).

4.3. Spectral power of the MU-ST

The beta log (SMPI) for MU-ST signals calculated with the coherence method is significantly greater than zero, in contrast to the other two methods in which the beta log (SMPI) does not significantly differ from zero. When comparing between methods of MU-ST spectral analysis, the difference in log (SMPI) is not significant after Bonferroni correction for multiple comparisons, but it does show a trend. Contrary to the LFP signal, the MU-ST analysis is not influenced by volume conduction in any of the methods. A way to explain the trend could be that the oscillations in the MU-ST signal that are coherent with the beta LFP can be caused by a summation of multiple oscillating neurons, leading to a larger peak in the PSD of the MU-ST signal. Because this summation of oscillating neurons in the MU-ST signal is more likely to occur in the sensorimotor STN where oscillating neurons are more abundant (Weinberger et al., 2006), the power of the MU-ST signal at the coherent frequencies is greater here than in the non-sensorimotor STN. This is in agreement with the finding that the beta log (SMPI) of MU-ST signals is significantly greater than zero when using the coherence methods, even though the percentage of measurements that show a significant coherence between LFP and MU-ST does not differ between sensorimotor and non-sensorimotor STN. The spectral analysis in the other two methods is probably influenced too much by other peaks in the PSD of the MU-ST signal, leading to an average log (SMPI) value which is not significantly greater than zero.

In gamma frequencies, no average log (SMPI) values significantly greater than zero were found for any of the methods and no significant differences were found between methods. Similar to the gamma LFP results, this may be explained by the fact that the measurements in this study were performed during rest. Previous research on oscillatory spiking activity has also found an equal distribution of gamma oscillations within the STN (Contarino et al., 2012).

4.4. Limitations and recommendations

In this study, we used a personalized atlas of the STN mapped on the intraoperative microelectrode recording sites to estimate the size and location of the sensorimotor and non-sensorimotor part of the STN. The subdivision of the STN in different functional areas, based on an atlas model is derived from histological studies, (Parent and Hazrati, 1995), and it might not be fitting with the true subdivision for each patient. Therefore, we can only use it as an estimate. Although such an estimate will not be sufficient to correctly guide electrode implantation, it is sufficient for this study to show the potential added value of the coherence method. We demonstrate that using this new method can be beneficial in locating the sensorimotor STN area for each patient specifically, so that electrode placement can in the future possibly be guided by beta LFP power and estimates based on atlas coordinates may no longer be necessary.

Analyzing the LFP power of only the specific coherent frequencies minimizes the influence of LFP oscillations from distant sites but it does not fully exclude it. The frequencies of distant LFP oscillations may overlap with the coherent frequencies and may therefore still add to the calculated LFP power. Often bipolar LFP recordings are used to minimize the effects of distant low frequency oscillations. However, intraoperative LFP recordings with a sufficient spatial resolution require extensive changes to the standard surgical procedures. The goal of this study was to intraoperatively localize the STN and its sensorimotor part without significant changes to the standard surgical procedures. The coherence method is used in this study as a way to do that by making the analysis of the LFP beta oscillations more local. However, many center are no longer using microelectrodes to guide DBS implantation. We therefore recommend to look for other methods that can measure the beta oscillations in the LFP very locally without extensive changes to the surgical procedures. Recent advances in technology have led to the development of DBS leads which deliver stimulation through multiple smaller contact points, ranging from 8 to 32 individual contacts (Contarino et al., 2014; Hariz, 2014; Martens et al., 2011; Pollo et al., 2014). These multi-contact arrays make it possible to do bipolar LFP recordings with a much better spatial resolution. Using this type of high resolution LFP recordings might make it possible to do advanced intraoperative target identification of the sensorimotor STN.

This study demonstrates significantly elevated LFP and MU-ST beta power on a group level. Furthermore, it shows that the discriminative ratio between sensorimotor and non-sensorimotor STN based on beta frequencies can be increased by using the coherence method. However, to proof that the coherence method truly preforms better than the other two methods in identifying the

sensorimotor STN, a difference between the methods should be shown at patient level. However, we found that this was not possible due to the limited number of measurement sites available per STN, especially in the non-sensorimotor STN. The median amount of measurement sites is 13 in the sensorimotor area and 6 in the non-sensorimotor area. Therefore, we chose to use the sensorimotor power index (SMPI) as a measure to express the ability to discriminate between sensorimotor and non-sensorimotor STN and compare the SMPI values between the three methods. We found that in 30 out of 44 STNs the SMPI value using the coherence method was greater than the SMPI values using the other two methods.

Although the coherence method performs better at group level, the limited number of available measurement sites per patient makes a comparison between methods at patient level unreliable. When a comparison at patient level was performed, we found that the distributions of beta powers in both the sensorimotor and the non-sensorimotor STN were skewed to the right. Therefore, we used log-transformation and independent samples *t*-tests to compare the beta powers in the sensorimotor STN with the beta powers in the non-sensorimotor STN, for all three methods. We found that using the coherence method, the beta power in the sensorimotor STN was significantly increased in only three out of 44 STNs. In both of the other two methods, we found a significant increase in only five out of 44 STNs. These numbers are too small to reliably compare the performance of the three methods at patient level.

5. Conclusion

In conclusion, the coherence method potentially has an added value for the discrimination of the sensorimotor STN, because of its ability to specifically analyze the power of locally measured beta oscillations. Volume conduction of beta frequency oscillations in the LFP signal interferes with the intraoperative identification of the sensorimotor STN and therefore it probably cannot be done with LFP recordings alone. However, for the use of the coherence method to discriminate the sensorimotor STN from the non-sensorimotor STN at patient level, more measurement sites per STN would be necessary. When these are available, simultaneous recordings of LFP and neuronal spiking activity could be beneficial in intraoperative target identification of the sensorimotor STN. With only a minor modification of standard surgical procedures, it is possible to increase the discrimination between measurements inside and outside the sensorimotor STN.

Acknowledgements

The authors would like to thank H. Martens and Sapiens Steering Brain Stimulation BV (now Medtronic Eindhoven Design Center) for their support in the supply of data acquisition hardware. Furthermore, we would like to thank the movement disorders nurses M. Scholten, M. Postma and G. Iwan for assistance with the patients.

References

Alavi M, Dostrovsky JO, Hodaie M, Lozano AM, Hutchison WD. Spatial extent of beta oscillatory activity in and between the subthalamic nucleus and substantia nigra pars reticulata of Parkinson's disease patients. Exp Neurol 2013;245:60–71.

Alegre M, Alonso-Frech F, Rodriguez-Oroz MC, Guridi J, Zamarbide I, Valencia M, et al. Movement-related changes in oscillatory activity in the human subthalamic nucleus: ipsilateral vs. contralateral movements. Eur J Neurosci 2005;22:2315–24.

Amirnovin R, Williams ZM, Cosgrove GR, Eskandar EN. Experience with microelectrode guided subthalamic nucleus deep brain stimulation. Neurosurgery 2006;58:ONS96–102.

Androulidakis AG, Kühn AA, Chen CC, Blomstedt P, Kempf F, Kupsch A, et al. Dopaminergic therapy promotes lateralized motor activity in the subthalamic area in Parkinson's disease. Brain 2007;130:457–68.

Bakstein E, Burgess J, Warwick K, Ruiz V, Aziz T, Stein J. Parkinsonian tremor identification with multiple local field potential feature classification. J Neurosci Methods 2012;209:320–30.

Benabid AL, Chabardes S, Mitrofanis J, Pollak P. Deep brain stimulation of the subthalamic nucleus for the treatment of Parkinson's disease. Lancet Neurol 2009;8:67–81.

Benarroch EE. Subthalamic nucleus and its connections: anatomic substrate for the network effects of deep brain stimulation. Neurology 2008;70:1991–5.

Bour LJ, Contarino MF, Foncke EM, de Bie RM, van den Munckhof P, Speelman JD, et al. Long-term experience with intraoperative microrecording during DBS neurosurgery in STN and GPi. Acta Neurochir (Wien) 2010;152:2069–77.

Brown P. Abnormal oscillatory synchronisation in the motor system leads to impaired movement. Curr Opin Neurobiol 2007;17:656–64.

Brown P. Oscillatory nature of human basal ganglia activity: relationship to the pathophysiology of Parkinson's disease. Mov Disord 2003;18:357–63.

Brown P, Eusebio A. Paradoxes of functional neurosurgery: clues from basal ganglia recordings. Mov Disord 2008;23:12–20.

Brown P, Williams D. Basal ganglia local field potential activity: character and functional significance in the human. Clin Neurophysiol 2005;116:2510–9 (Official Journal of the International Federation of Clinical Neurophysiology).

Butson CR, Cooper SE, Henderson JM, McIntyre CC. Patient-specific analysis of the volume of tissue activated during deep brain stimulation. NeuroImage 2007;34:661–70.

Buzsaki G. Theta oscillations in the hippocampus. Neuron 2002;33:325–40.

Buzsaki G, Anastassiou CA, Koch C. The origin of extracellular fields and currents—EEG, ECoG, LFP and spikes. Nat Rev Neurosci 2012;13:407–20.

Cagnan H, Dolan K, He X, Contarino MF, Schuurman R, van den Munckhof P, et al. Automatic subthalamic nucleus detection from microelectrode recordings based on noise level and neuronal activity. J Neural Eng 2011;8:046006.

Cassidy M, Mazzone P, Oliviero A, Insola A, Tonali P, Di Lazzaro V, et al. Movement-related changes in synchronization in the human basal ganglia. Brain 2002;125:1235–46.

Chen CC, Pogosyan A, Zrinzo LU, Tisch S, Limousin P, Ashkan K, et al. Intra-operative recordings of local field potentials can help localize the subthalamic nucleus in Parkinson's disease surgery. Exp Neurol 2006;198:214–21.

Contarino MF, Bour LJ, Bot M, van den Munckhof P, Speelman JD, Schuurman PR, et al. Tremor-specific neuronal oscillation pattern in dorsal subthalamic nucleus of parkinsonian patients. Brain Stimul 2012;5:305–14.

Contarino MF, Bour LJ, Verhagen R, Lourens MA, de Bie RM, van den Munckhof P, et al. Directional steering: a novel approach to deep brain stimulation. Neurology 2014;83:1163–9.

Deuschl G, Schade-Brittinger C, Krack P, Volkmann J, Schafer H, Botzel K, et al. A randomized trial of deep-brain stimulation for Parkinson's disease. N Engl J Med 2006;355:896–908.

Dolan K, Martens HC, Schuurman PR, Bour LJ. Automatic noise-level detection for extra-cellular micro-electrode recordings. Med Biol Eng Comput 2009;47:791–800.

Eusebio A, Cagnan H, Brown P. Does suppression of oscillatory synchronisation mediate some of the therapeutic effects of DBS in patients with Parkinson's disease? Front Integr Neurosci 2012;6:47.

Fogelson N, Pogosyan A, Kühn AA, Kupsch A, van Bruggen G, Speelman H, et al. Reciprocal interactions between oscillatory activities of different frequencies in the subthalamic region of patients with Parkinson's disease. Eur J Neurosci 2005;22:257–66.

Goto Y, O'Donnell P. Network synchrony in the nucleus accumbens in vivo. J Neurosci 2001;21:4498–504.

Grover FS, Buchwald JS. Correlation of cell size with amplitude of background fast activity in specific brain nuclei. J Neurophysiol 1970;33:160–71.

Halliday DM, Rosenberg JR, Amjad AM, Breeze P, Conway BA, Farmer SF. A framework for the analysis of mixed time series/point process data—theory and application to the study of physiological tremor, single motor unit discharges and electromyograms. Prog Biophys Mol Biol 1995;64:237–78.

Hamani C, Saint-Cyr JA, Fraser J, Kaplitt M, Lozano AM. The subthalamic nucleus in the context of movement disorders. Brain 2004;127:4–20.

Hariz M. Deep brain stimulation: new techniques. Parkinsonism Relat Disord 2014;20(Suppl. 1):S192–6.

Henze DA, Borhegyi Z, Csicsvari J, Mamiya A, Harris KD, Buzsaki G. Intracellular features predicted by extracellular recordings in the hippocampus in vivo. J Neurophysiol 2000;84:390–400.

Jenkinson N, Brown P. New insights into the relationship between dopamine, beta oscillations and motor function. Trends Neurosci 2011;34:611–8.

Juergens E, Guettler A, Eckhorn R. Visual stimulation elicits locked and induced gamma oscillations in monkey intracortical- and EEG-potentials, but not in human EEG. Exp Brain Res 1999;129:247–59.

Kajikawa Y, Schroeder CE. How local is the local field potential? Neuron 2011;72:847–58.

Kühn AA, Kupsch A, Schneider GH, Brown P. Reduction in subthalamic 8–35 Hz oscillatory activity correlates with clinical improvement in Parkinson's disease. Eur J Neurosci 2006;23:1956–60.

Kühn AA, Trottenberg T, Kivi A, Kupsch A, Schneider GH, Brown P. The relationship between local field potential and neuronal discharge in the subthalamic nucleus of patients with Parkinson's disease. Exp Neurol 2005;194:212–20.

Legatt AD, Arezzo J, Vaughan HG Jr. Averaged multiple unit activity as an estimate of phasic changes in local neuronal activity: effects of volume-conducted potentials. J Neurosci Methods 1980;2:203–17.

Linden H, Pettersen KH, Einevoll GT. Intrinsic dendritic filtering gives low-pass power spectra of local field potentials. J Comput Neurosci 2010;29:423–44.
Little S, Pogosyan A, Neal S, Zavala B, Zrinzo L, Hariz M, et al. Adaptive deep brain stimulation in advanced Parkinson disease. Ann Neurol 2013;74:449–57.
Logothetis NK. The neural basis of the blood-oxygen-level-dependent functional magnetic resonance imaging signal. Philos Trans R Soc London B: Biol Sci 2002;357:1003–37.
Logothetis NK. The underpinnings of the BOLD functional magnetic resonance imaging signal. J Neurosci 2003;23:3963–71.
Lourens MA, Meijer HG, Contarino MF, van den Munckhof P, Schuurman PR, van Gils SA, et al. Functional neuronal activity and connectivity within the subthalamic nucleus in Parkinson's disease. Clin Neurophysiol 2013;124:967–81.
Lujan JL, Noecker AM, Butson CR, Cooper SE, Walter BL, Vitek JL, et al. Automated 3-dimensional brain atlas fitting to microelectrode recordings from deep brain stimulation surgeries. Stereotact Funct Neurosurg 2009;87:229–40.
Mallet L, Schupbach M, N'Diaye K, Remy P, Bardinet E, Czernecki V, et al. Stimulation of subterritories of the subthalamic nucleus reveals its role in the integration of the emotional and motor aspects of behavior. Proc Natl Acad Sci USA 2007;104:10661–6.
Martens HC, Toader E, Decre MM, Anderson DJ, Vetter R, Kipke DR, et al. Spatial steering of deep brain stimulation volumes using a novel lead design. Clin Neurophysiol 2011;122:558–66 (Official Journal of the International Federation of Clinical Neurophysiology).
Miocinovic S, Noecker AM, Maks CB, Butson CR, McIntyre CC. Cicerone: stereotactic neurophysiological recording and deep brain stimulation electrode placement software system. Acta Neurochir Suppl 2007;97:561–7.
Mitzdorf U. Properties of the evoked potential generators: current source-density analysis of visually evoked potentials in the cat cortex. Int J Neurosci 1987;33:33–59.
Moran A, Bar-Gad I. Revealing neuronal functional organization through the relation between multi-scale oscillatory extracellular signals. J Neurosci Methods 2010;186:116–29.
Odekerken VJ, van Laar T, Staal MJ, Mosch A, Hoffmann CF, Nijssen PC, et al. Subthalamic nucleus versus globus pallidus bilateral deep brain stimulation for advanced Parkinson's disease (NSTAPS study): a randomised controlled trial. Lancet Neurol 2013;12:37–44.
Parent A, Hazrati LN. Functional anatomy of the basal ganglia. II. The place of subthalamic nucleus and external pallidum in basal ganglia circuitry. Brain Res Brain Res Rev 1995;20:128–54.
Pedemonte M, Barrenechea C, Nunez A, Gambini JP, Garcia-Austt E. Membrane and circuit properties of lateral septum neurons: relationships with hippocampal rhythms. Brain Res 1998;800:145–53.
Pollo C, Kaelin-Lang A, Oertel MF, Stieglitz L, Taub E, Fuhr P, et al. Directional deep brain stimulation: an intraoperative double-blind pilot study. Brain 2014;137:2015–26.
Priori A, Foffani G, Rossi L, Marceglia S. Adaptive deep brain stimulation (aDBS) controlled by local field potential oscillations. Clin Exp Neurol 2013;245:77–86.
Saint-Cyr JA, Hoque T, Pereira LC, Dostrovsky JO, Hutchison WD, Mikulis DJ, et al. Localization of clinically effective stimulating electrodes in the human subthalamic nucleus on magnetic resonance imaging. J Neurosurg 2002;97:1152–66.
Schlaier JR, Habermeyer C, Janzen A, Fellner C, Hochreiter A, Proescholdt M, et al. The influence of intraoperative microelectrode recordings and clinical testing on the location of final stimulation sites in deep brain stimulation for Parkinson's disease. Acta Neurochir (Wien) 2013;155:357–66.
Temel Y, Blokland A, Steinbusch HW, Visser-Vandewalle V. The functional role of the subthalamic nucleus in cognitive and limbic circuits. Prog Neurobiol 2005;76:393–413.
Temel Y, Kessels A, Tan S, Topdag A, Boon P, Visser-Vandewalle V. Behavioural changes after bilateral subthalamic stimulation in advanced Parkinson disease: a systematic review. Parkinsonism Relat Disord 2006;12:265–72.
Trottenberg T, Fogelson N, Kühn AA, Kivi A, Kupsch A, Schneider GH, et al. Subthalamic gamma activity in patients with Parkinson's disease. Exp Neurol 2006;200:56–65.
Trottenberg T, Kupsch A, Schneider GH, Brown P, Kühn AA. Frequency-dependent distribution of local field potential activity within the subthalamic nucleus in Parkinson's disease. Exp Neurol 2007;205:287–91.
Ulla M, Thobois S, Llorca PM, Derost P, Lemaire JJ, Chereau-Boudet I, et al. Contact dependent reproducible hypomania induced by deep brain stimulation in Parkinson's disease: clinical, anatomical and functional imaging study. J Neurol Neurosurg Psychiatry 2011;82:607–14.
Voges J, Volkmann J, Allert N, Lehrke R, Koulousakis A, Freund HJ, et al. Bilateral high-frequency stimulation in the subthalamic nucleus for the treatment of Parkinson disease: correlation of therapeutic effect with anatomical electrode position. J Neurosurg 2002;96:269–79.
Weaver FM, Follett K, Stern M, Hur K, Harris C, Marks WJ Jr, et al. Bilateral deep brain stimulation vs best medical therapy for patients with advanced Parkinson disease: a randomized controlled trial. JAMA 2009;301:63–73.
Weinberger M, Hutchison WD, Lozano AM, Hodaie M, Dostrovsky JO. Increased gamma oscillatory activity in the subthalamic nucleus during tremor in Parkinson's disease patients. J Neurophysiol 2009;101:789–802.
Weinberger M, Mahant N, Hutchison WD, Lozano AM, Moro E, Hodaie M, et al. Beta oscillatory activity in the subthalamic nucleus and its relation to dopaminergic response in Parkinson's disease. J Neurophysiol 2006;96:3248–56.
Williams D, Tijssen M, van Bruggen G, Bosch A, Insola A, Di Lazzaro V, et al. Dopamine-dependent changes in the functional connectivity between basal ganglia and cerebral cortex in humans. Brain 2002;125:1558–69.
Winestone JS, Zaidel A, Bergman H, Israel Z. The use of macroelectrodes in recording cellular spiking activity. J Neurosci Methods 2012;206:34–9.
Witt K, Daniels C, Reiff J, Krack P, Volkmann J, Pinsker MO, et al. Neuropsychological and psychiatric changes after deep brain stimulation for Parkinson's disease: a randomised, multicentre study. Lancet Neurol 2008;7:605–14.
Yelnik J, Damier P, Demeret S, Gervais D, Bardinet E, Bejjani BP, et al. Localization of stimulating electrodes in patients with Parkinson disease by using a three-dimensional atlas-magnetic resonance imaging coregistration method. J Neurosurg 2003;99:89–99.